ACTA CHEMICA SCANDINAVICA 21 (1967) 513–526

On the Structural Properties of the $Ta_{1+x}Se_2$ Phase

EINAR BJERKELUND and ARNE KJEKSHUS

Kjemisk Institutt A, Universitetet i Oslo, Blindern, Oslo 3, Norway

The $Ta_{1+x}Se_2$ phase has been studied by X-ray diffraction, density, and magnetic susceptibility measurements. The $Ta_{1+x}Se_2$ phase has a homogeneity range within the limits 55.0 and 66.67 atomic % Se. Six polytype modifications $1T$, $2H$, $3R$, $4H_{(a)}$, $4H_{(b)}$, and $6R$ of the $Ta_{1+x}Se_2$ phase have been observed. The results are discussed in relation to those reported by previous investigators of this phase.

A survey of the literature shows that tantalum selenides were described for the first time in 1956 by Ariya *et al.*[1] The history of the Ta-Se system is thus short compared with that of some of the other chalcogen systems of the transition metals which have been subjected to frequent investigations over a period of more than 150 years. However, the last decennium has seen considerable activity, with several publications on structural, electrical, thermoelectrical, lubricating, and magnetic properties of the intermediate tantalum selenide phases. A comprehensive list of references to these papers is included in a recent description[2] of the phase relationships in the Ta-Se system.

In the Ta-Se system the existence of one phase with a wide range of homogeneity has been established.[1–11] The present paper concerns the range of homogeneity and some of the structural and magnetic properties of this phase, which has been designated $Ta_{1+x}Se_2$. The important stages in the development of our knowledge on the $Ta_{1+x}Se_2$ phase may be listed as:

(1) The establishment of its existence and the recognition of a homogeneity range by Ariya *et al.*[1]

(2) The identification of two polytypes of $TaSe_2$ by Brixner.[3]

(3) The determinations of the crystal structures of in all five polytypes of $TaSe_2$ by Kadijk *et al.*[8] and/or Brown and Beerntsen.[9]

EXPERIMENTAL

Materials. The tantalum metal used in this study was "Spectrographically standardized tantalum" obtained from Johnson, Matthey & Co., Ltd. According to the supplied analysis it contained the following impurities (in ppm): Mg(1), Al(20), Si(100), Cr(20), Mn(5), Nb(<200), and Sn(20). (A Guinier photograph of the tantalum metal gave a

lattice constant of 3.3067 Å, in close agreement with the value 3.3058 Å reported by Swanson and Tatge.[12] The highly purified selenium was a gift from Bolidens Gruvaktiebolag, Sweden. It carried the analysis (in ppm): Na(0.4), K(0.3), Fe(0.8), Cu(2), and non-volatile matter (12).

Preparations. Samples having the compositions 44.44, 45.95, 47.37, 48.72, 50.00, 52.38, 54.55, 55.56, 56.52, 58.33, 59.18, 60.00, 62.26, 62.96, 63.64, 64.29, 66.10, 66.33, 66.67, 67.00, 69.23, and 71.43 atomic % Se were prepared by heating weighed quantities of the components in evacuated and sealed silica tubes. In some cases crucibles of pure alumina were placed inside the silica tubes. All samples were first heated at 900°C for 14 days and cooled slowly to room temperature over a period of 20 days. The samples were afterwards crushed and reannealed at various temperatures between 200 and 900°C and finally quenched in ice water or cooled slowly to room temperature.

It proved to be rather difficult to obtain consistent, reproducible results for samples containing less than ~66.7 atomic % Se. A part of this difficulty arises from the presence of an apparently unavoidable interfering reaction between Ta and SiO_2 (easily observable < 54 atomic % Se). The effects of this reaction can be reduced (but not eliminated) by placing the samples in alumina crucibles inside the silica tubes. The contamination is quite variable, even for samples with the same initial composition. The results obtained on highly contaminated samples are not included in this paper. (See also Selte *et al.*[2])

X-Ray diffraction. All samples were crushed and X-ray photographs were taken in a Guinier type focusing camera of 80 mm diameter using strictly monochromatized Cu$K\alpha_1$-radiation. Potassium chloride (Analar, The British Drug Houses, Ltd. a = 6.2919 Å [13]) was added to the specimen as an internal standard. Lattice dimensions, which are expressed in Ångström units on the basis of $\lambda(\mathrm{Cu}K\alpha_1) = 1.54050$ Å, were refined by applying the method of least squares to the Guinier photographic data. The indicated error limits correspond to twice the standard deviations obtained in these calculations.

Some X-ray photographs were also taken with a Weissenberg camera of 57.3 mm diameter using Cu$K\alpha$-radiation.

Density measurements. The density measurements were carried out pycnometrically at 25°C with kerosene as displacement liquid. To remove gases adsorbed by the sample (approx. 2 g) the pycnometer was filled with kerosene under vacuum.

Magnetic measurements. The magnetic susceptibilities were measured by the Gouy method at three different maximum field strengths (H_{max} = 4015, 4700, and 5110 Ø). The samples were enclosed in evacuated and sealed silica tubes of 3 mm internal diameter to a height of about 85 mm.

RESULTS AND DISCUSSION

(i) *Polytypes of $TaSe_2$.* The presentation of the $Ta_{1+x}Se_2$ phase starts conveniently with the results obtained for $TaSe_2$, *i.e.* the composition for $x = 0.00$ which corresponds to the selenium-rich phase limit.

$TaSe_2$ crystallizes in at least six closely-related structures of the layer type. The rational nomenclature adopted for naming the different polytypes of $TaSe_2$ follows that previously used by Brown and Beerntsen.[9] This scheme of notation uses a prefix added to the formula in order to distinguish and designate the various polytypes. The first part of this prefix is an integer which corresponds to half the number of Se layers per unit length of the c axis. The second part of the prefix is a letter which gives the symmetry of the unit cell (T = trigonal, H = hexagonal, and R = rhombohedral). To differentiate between different polytypes with equal numbers of Se layers and equal crystal symmetry, a letter subscript in parentheses is included as a third part of the prefix.

Six polytypes of $TaSe_2$ have been observed, *i.e.* $1T$-$TaSe_2$, $2H$-$TaSe_2$, $3R$-$TaSe_2$, $4H_{(a)}$-$TaSe_2$, $4H_{(b)}$-$TaSe_2$, and $6R$-$TaSe_2$; and X-ray powder data for their characterization are given in Tables 1—6. (It should be noted that the intensities listed for some of the reflections of the type $00l$ may suffer from the effect of preferred orientation.)

Table 1. Guinier photographic data of 1*T*-$TaSe_2$ taken with Cu$K\alpha_1$-radiation.

I_{obs}	$\sin^2\theta \times 10^5$		*hkl*	I_{obs}	$\sin^2\theta \times 10^5$		*hkl*
	obs	calc			obs	calc	
m	1 510	1 509	001	m	21 139	21 139	111
m	6 551	6 543	100	vw	24 124	24 129	004
vst	8 050	8 052	101	vw	26 173	26 173	200
m	12 578	12 575	102	m	27 686	27 682	201
vw	13 578	13 572	003	w	32 204	32 208	202
vst	19 624	19 631	110	vw	33 195	33 203	113
w	20 115	20 115	103				

Table 2. Guinier photographic data of 2*H*-$TaSe_2$ taken with Cu$K\alpha_1$-radiation.

I_{obs}	$\sin^2\theta \times 10^5$		*hkl*	I_{obs}	$\sin^2\theta \times 10^5$		*hkl*
	obs	calc			obs	calc	
st	1 474	1 473	002	m	21 572	21 572	112
w	6 705	6 701	100	vw	23 560	23 556	008
st	7 070	7 068	101	w	26 800	26 800	200
vst	8 176	8 174	102	w	27 168	27 168	201
w	10 011	10 013	103	m	28 282	28 274	202
st	12 590	12 590	104	w	32 686	32 690	204
vw	13 239	13 251	006	vw	33 367	33 351	116
st	20 094	20 101	110				

Table 3. Guinier photographic data of 3*R*-$TaSe_2$ taken with Cu$K\alpha_1$-radiation. (The indices are given in terms of hexagonal axes.)

I_{obs}	$\sin^2\theta \times 10^5$		*hkl*	I_{obs}	$\sin^2\theta \times 10^5$		*hkl*
	obs	calc			obs	calc	
vst	1 457	1 452	003	vw	26 986	26 982	201
m	6 870	6 865	101	vw	27 464	27 464	202
w	7 359	7 350	102	vw	29 424	29 400	204
m	9 284	9 287	104	vw	30 830	30 854	205
m	10 729	10 737	105	m	33 203	33 182	119
w	13 065	13 068	009	vw	34 703	34 724	207
w	14 614	14 611	107	w	43 366	43 344	1,1,12
w	17 023	17 029	108	vw	47 096	47 096	211
st	20 119	20 115	110	vw	48 390	48 386	213
m	21 568	21 568	113	w	49 503	49 516	214
w	23 231	23 231	0,0,12				

Table 4. Guinier photographic data of $4H_{(a)}$-$TaSe_2$ taken with Cu$K\alpha_1$-radiation.

I_{obs}	$\sin^2\theta \times 10^5$		hkl	I_{obs}	$\sin^2\theta \times 10^5$		hkl
	obs	calc			obs	calc	
vst	1 463	1 472	004	vw	24 730	24 725	1,0,14
m	6 697	6 699	100	m	26 810	26 797	200
w	6 793	6 791	101	m	27 166	27 165	202
w	7 072	7 068	102	w	27 626	27 628	203
w	7 531	7 528	103	m	28 268	28 270	204
st	8 174	8 171	104	vw	29 113	29 099	205
w	9 002	9 000	105	vw	31 280	31 306	207
m	10 005	10 011	106	w	32 676	32 686	208
w	11 211	11 206	107	st	33 351	33 343	1,1,12
m	12 578	12 587	108	vw	36 533	36 499	1,0,18
vw	13 248	13 242	0,0,12	st	43 647	43 642	1,1,16
vw	14 124	14 148	109	w	46 898	46 895	210
vw	15 910	15 897	1,0,10	m	47 247	47 266	212
vst	20 098	20 098	110	vw	47 784	47 753	213
st	21 561	21 572	114	m	48 354	48 368	214
m	23 401	23 408	116	w	49 213	49 197	215

Table 5. Guinier photographic data of $4H_{(b)}$-$TaSe_2$ taken with Cu$K\alpha_1$-radiation.

I_{obs}	$\sin^2\theta \times 10^5$		hkl	I_{obs}	$\sin^2\theta \times 10^5$		hkl
	obs	calc			obs	calc	
st	1 506	1 501	004	vw	26 565	26 561	201
m	6 623	6 618	100	w	27 308	27 312	203
w	6 712	6 712	101	m	27 964	27 972	204
st	7 464	7 462	103	w	28 822	28 814	205
vst	8 121	8 119	104	vw	30 620	30 640	1,0,16
m	8 967	8 962	105	vw	31 059	31 068	207
w	11 217	11 217	107	m	32 473	32 473	208
vst	12 619	12 625	108	w	33 347	33 367	1,1,12
w	13 507	13 513	0,0,12	vw	37 832	37 823	2,0,11
st	19 850	19 850	110	w	39 989	39 985	2,0,12
w	20 122	20 133	1,0,12	vw	42 359	42 329	2,0,13
m	21 368	21 353	114	m	43 889	43 876	1,1,16
w	22 465	22 476	1,0,13	w	44 175	44 158	1,0,20
w	26 457	26 469	200	vw	46 395	46 412	211

With the exception of $1T$-$TaSe_2$ (see below), the crystal structures of these polytypes have been determined by Kadijk *et al.*[8] and/or Brown and Beerntsen.[9] The structure types, space groups, and the atomic arrangement of the various polytypes are listed in Table 7 and their unit cell dimensions are given in Table 8. Brief considerations and comments on the crystal structures (see Fig. 1) are presented below.

Table 6. Guinier photographic data of $6R$-$TaSe_2$ taken with Cu$K\alpha_1$-radiation. (The indices are given in terms of hexagonal axes.)

I_{obs}	$\sin^2\theta \times 10^5$		hkl	I_{obs}	$\sin^2\theta \times 10^5$		hkl
	obs	calc			obs	calc	
vst	1 498	1 493	006	m	21 357	21 364	116
m	6 664	6 666	101	vw	21 597	21 593	1,0,19
m	6 793	6 791	102	vw	23 216	23 209	1,0,20
st	7 286	7 288	104	m	23 875	23 883	0,0,24
w	7 669	7 660	105	w	26 530	26 538	201
vst	8 658	8 656	107	w	26 661	26 661	202
w	9 279	9 276	108	w	27 145	27 161	204
w	10 772	10 769	1,0,10	vw	27 530	27 534	205
st	11 647	11 642	1,0,11	m	28 530	28 526	207
m	13 429	13 435	0,0,18	vw	29 149	29 150	208
st	13 632	13 632	1,0,13	vw	30 656	30 640	2,0,10
vw	14 750	14 750	1,0,14	m	31 521	31 513	2,0,11
vw	17 237	17 240	1,0,16	vw	32 555	32 539	1,0,25
m	18 605	18 609	1,0,17	m	33 306	33 306	1,1,18
st	19 867	19 871	110	w	33 499	33 503	2,0,13

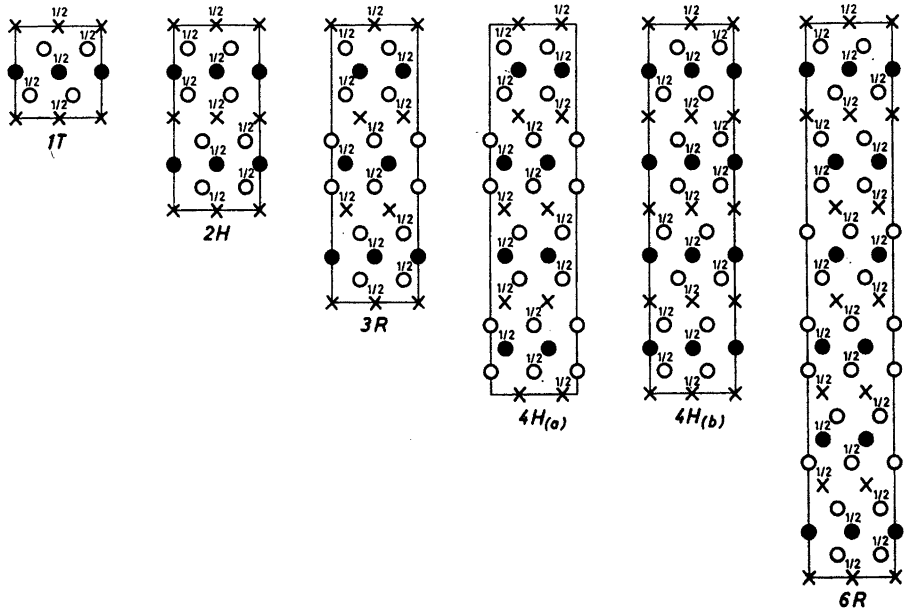

Fig. 1. The crystal structures of the six polytype modifications $1T$, $2H$, $3R$, $4H_{(a)}$, $4H_{(b)}$, and $6R$ of the $Ta_{1+x}Se_2$ phase projected along [100] of the orthohexagonal unit cells. (Equivalent to projection along [110] of the hexagonal unit cells.) The numbers indicate fractions of the projection axes. Filled circles represent Ta atoms and open circles Se atoms. Crosses indicate the positions of partially filled lattice sites (when $x > 0$ in $Ta_{1+x}Se_2$). For the polytype $1T$ the origin of this diagram is shifted to 0,0,1/2, for $3R$ to 0,0,5/6, and for $4H_{(a)}$ and $4H_{(b)}$ to 0,0,1/8 compared with Table 7.

Table 7. Crystallographic description of the polytype modifications of the $Ta_{1+x}Se_2$ phase.

Notation	1*T*	2*H*	3*R*
Structure prototype	$Cd(OH)_2$	2*H*-NbS_2	3*R*-MoS_2
Space group	$P\bar{3}m1$	$P6_3/mmc$	$R3m$ (Hexagonal description)
Coordinates	$1Ta_I$ in (*a*) $2Se$ in (*d*); $z \approx 1/4$	$2Ta_I$ in (*b*) $4Se$ in (*f*); $z \approx 1/8$	$3Ta_I$ in (*a*); $z = 0$ $3Se_I$ in (*a*); $z \approx 1/4$ $3Se_{II}$ in (*a*); $z \approx 5/12$
	$x Ta_{II}$ in (*b*)	$2x Ta_{II}$ in (*a*)	$3x Ta_{II}$ in (*a*); $z \approx 5/6$

1*T*-$TaSe_2$ crystallizes with the $Cd(OH)_2$ type structure, *cf.* Table 7 and Fig. 1. The value of the variable *z*-parameter was estimated to be 0.25 ± 0.01 (*i.e.* close to its "ideal" value $z = 1/4$) by comparing observed and calculated intensities of the Guinier photographs. 1*T*-$TaSe_2$ is a polytype of $TaSe_2$, hitherto unobserved, with a possible exception of an indefinite statement regarding a sub-lattice of appropriate dimensions (see Table 8) mentioned by Aslanov *et al.*[5] It is interesting to observe that Kadijk *et al.*[8] have predicted that 1*T*-$TaSe_2$ (with $Cd(OH)_2$ type structure and octahedral coordination around Ta) is likely to be non-existent. This prediction is based on Jellinek's rule [14] for TX_2 layer structures which states that: Layer structures with trigonal prismatic coordination around the metal atoms form if c/a exceeds a critical value of about $1.78 \times n$, whereas for smaller values of c/a octahedral coordination around the metal atoms is found. (n corresponds to half the number of non-metal atom layers within the unit repeat distance along the *c* axis, *i.e.* to the integer in the first part of the prefix to the chemical formula.) The structure of 1*T*-$TaSe_2$ with $c/a = 1.804$ is thus an exception to Jellinek's rule. Jellinek's [14] considerations are based on the assumption of rigid, spheric symmetric atoms (*i.e.* atoms with definite radii). This idealized assumption is shown to be only a first approximation and the failure of the rule is thus not very surprising. However, it is interesting to observe that 1*T*-$TaSe_2$ is a rather unstable high-temperature phase which has only been obtained in samples quenched from 900°C using a very high quenching rate.

2*H*-$TaSe_2$ is isostructural with 2*H*-NbS_2 (Fig. 1) according to structure determinations reported by Kadijk *et al.*[8] and Brown and Beerntsen.[9] The

(The lattice dimensions are listed in Table 8.)

$4H_{(a)}$	$4H_{(b)}$	$6R$
$4H_{(a)}$-$NbSe_2$	$4H_{(b)}$-$TaSe_2$	$6R$-TaS_2
$P\bar{6}m2$	$P6_3/mmc$	$R3m$ (Hexagonal description)
$1Ta_I$ in (c) $1Ta_{II}$ in (f) $2Ta_{III}$ in (i); $z \approx 1/4$ $2Se_I$ in (i); $z \approx 1/16$ $2Se_{II}$ in (g); $z \approx 3/16$ $2Se_{III}$ in (g); $z \approx 5/16$ $2Se_{IV}$ in (h); $z \approx 7/16$	$2Ta_I$ in (a) $2Ta_{II}$ in (b) $4Se_I$ in (f); $z \approx 1/16$ $4Se_{II}$ in (f); $z \approx 11/16$	$3Ta_I$ in (a); $z = 1/12$ $3Ta_{II}$ in (a); $z \approx 11/12$ $3Se_I$ in (a); $z \approx 5/24$ $3Se_{II}$ in (a); $z \approx 3/8$ $3Se_{III}$ in (a); $z \approx 11/24$ $3Se_{IV}$ in (a); $z \approx 5/8$
$2x_1Ta_{IV}$ in (h); $z \approx 1/8$ $2x_2Ta_V$ in (i); $z \approx 3/8$	$4xTa_{III}$ in (e); $z \approx 1/8$	$3x_1Ta_{III}$ in (a); $z \approx 0$ $3x_2Ta_{IV}$ in (a); $z \approx 5/6$

proposed structure has also been confirmed in the present study by means of X-ray methods applied to single crystals. Well formed, plate like single crystals of hexagonal shape were investigated using a Weissenberg goniometer with the rotation axis along the hexagonal axis. (Intensity measurements were carried out visually.) The best agreement (judged from a minimum of $R = \sum||F_o|-|F_c||/\sum|F_o|$) between observed and calculated structure factors was obtained for the parameter value $z = 0.125 \pm 0.005$. This value differs somewhat from the value $z = 0.118 \pm 0.001$ reported by Brown and Beerntsen,[9] but no explanation can be suggested to resolve the discrepancy. $2H$-$TaSe_2$ has probably been prepared in all the previous studies[1-11] of the $Ta_{1+x}Se_2$ phase. The best conditions for the preparation of this polytype may be suggested as heat treatment at ~800°C followed by slow-cooling to room temperature.

The crystal structures of $3R$-$TaSe_2$, $4H_{(a)}$-$TaSe_2$, $4H_{(b)}$-$TaSe_2$, and $6R$-$TaSe_2$ (*cf.* Table 7 and Fig. 1) have been inferred from pronounced similarities in lattice dimensions (Table 8) and diffraction data when compared with the corresponding data reported by Kadijk *et al.*[8] or Brown and Beerntsen.[9] The correspondences seem close enough to confirm the structural identity in each case, but no attempts have been made to refine the variable z-parameters. Our purest samples of $3R$-$TaSe_2$ (containing small amounts of $2H$-$TaSe_2$ as impurity) have been obtained by heat treatment of $1T$-$TaSe_2$ at 300—500°C. (Kadijk *et al.* report the preparation of pure $3R$-$TaSe_2$ at 500—600°C.) $4H_{(a)}$-$TaSe_2$ has been prepared by protracted annealing of the samples at 900°C followed by slow-cooling to room temperature. $4H_{(b)}$-$TaSe_2$ and $6R$-$TaSe_2$

Table 8. Unit cell dimensions of the $Ta_{1+x}Se_2$ phase.

Composition		Poly-type	Lattice dimensions				Ref.
At. % Se	x		a (Å)	c (Å)	c/a	V (Å^3)	
55.56	0.60	2*H*	3.430 ±0.001	13.00 ±0.01	2 × 1.895	132.41	
56.52	0.54	2*H*	3.429 ±0.001	12.97 ±0.01	2 × 1.890	132.04	
58.33	0.43	2*H*	3.432 ±0.001	12.92 ±0.01	2 × 1.882	131.71	
59.18	0.38	2*H*	3.433 ±0.001	12.89 ±0.01	2 × 1.877	131.52	
60.00	0.33	2*H*	3.434 ±0.001	12.87 ±0.01	2 × 1.874	131.46	
62.26	0.21	3*R*	3.444 ±0.001	18.88 ±0.02	3 × 1.827	193.98	
62.96	0.18	3*R*	3.444 ±0.001	18.91 ±0.02	3 × 1.830	194.18	
63.64	0.14	3*R*	3.443 ±0.001	18.93 ±0.02	3 × 1.832	194.24	
64.29	0.11	3*R*	3.442 ±0.001	18.98 ±0.02	3 × 1.838	194.69	
66.10	0.03	3*R*	3.437 ±0.001	19.05 ±0.02	3 × 1.848	194.88	
66.33	0.02	2*H*	3.437 ±0.001	12.694 ±0.005	2 × 1.846	129.89	
66.67	0.00	1*T*	3.4769±0.0004	6.2722±0.0016	1.804	65.66	
66.67	0.00	2*H*	3.4360±0.0003	12.696 ±0.004	2 × 1.847	129.80	
66.67	0.00	3*R*	3.4348±0.0004	19.177 ±0.004	3 × 1.861	195.94	
66.67	0.00	$4H_{(a)}$	3.4362±0.0004	25.399 ±0.009	4 × 1.848	259.72	
66.67	0.00	$4H_{(b)}$	3.4575±0.0004	25.143 ±0.005	4 × 1.818	260.30	
66.67	0.00	6*R*	3.4558±0.0003	37.826 ±0.007	6 × 1.824	391.22	
50.00	1.00	2*H*	3.425 ±0.005	12.746 ±0.005	2 × 1.861	129.49	3
66.67	0.00	2*H*	3.431 ±0.005	12.737 ±0.005	2 × 1.856	129.85	3
66.67	0.00	3*R*	3.428 ±0.005	19.100 ±0.005	3 × 1.857	194.37	3
66.67	0.00	3*R*	3.446	19.101	3 × 1.848	196.43	4
66.44	0.01	2*H*	3.429	12.73	2 × 1.856	129.6	5
66.44	0.01	6*R*	3.46	37.9	6 × 1.83	392.7	5
66.67	0.00	"1*T*"	3.44	6.27	1.823	64.3	5
61.98	0.23	2*H*	3.439 ±0.001	12.963 ±0.005	2 × 1.885	132.77	6
62.55	0.20	2*H*	3.437 ±0.001	12.91 ±0.005	2 × 1.875	132.07	6
62.55	0.20	3*R*	3.437 ±0.001	18.82 ±0.01	3 × 1.830	192.53	6
66.44	0.01	2*H*	3.429 ±0.001	12.73 ±0.005	2 × 1.855	129.63	6
66.44	0.01	3*R*	3.429 ±0.001	19.11 ±0.01	3 × 1.857	194.59	6
66.67	0.00	2*H*	3.431	12.737	2 × 1.856	129.73	7
66.67	0.00	2*H*	3.437	12.72	2 × 1.851	130.2	8
66.67	0.00	3*R*	3.437	19.21	3 × 1.863	196.5	8
66.67	0.00	$4H_{(a)}$	3.43	25.5	4 × 1.86	240	8
66.67	0.00	6*R*	3.455	37.77	6 × 1.822	390.6	8
66.67	0.00	2*H*	3.43 ±0.01	12.71 ±0.04	2 × 1.852	129.4	9
66.67	0.00	$4H_{(b)}$	3.46 ±0.01	25.18 ±0.04	4 × 1.819	260.8	9
66.67	0.00	2*H*	3.43	12.71	2 × 1.852	129.4	10
66.67	0.00	$4H_{(b)}$	3.46	25.18	4 × 1.819	260.8	10
65.75	0.04	2*H*	3.430 ±0.002	12.71 ±0.01	2 × 1.853	129.38	11

have both been obtained as pure (or almost pure) phases in samples quenched from ~800°C.

Transition metal di-chalcogenides which have been reported to be isostructural with the various polytypes of $TaSe_2$ are listed in Table 9. $4H_{(b)}$-$TaSe_2$ appears to be the only one of these polytypes which has a unique crystal structure.

Table 9. Isostructural phases with the various polytypes of $TaSe_2$.

Polytype	Isostructural phases
1*T*-$TaSe_2$	TiS_2, $TiSe_2$, $TiTe_2$, ZrS_2, $ZrSe_2$, $ZrTe_2$, HfS_2, $HfSe_2$, TaS_2, $RhTe_2$, $IrTe_2$, $NiTe_2$, $PdTe_2$, PtS_2, $PtSe_2$, $PtTe_2$
2*H*-$TaSe_2$	NbS_2, $NbSe_2$, TaS_2
3*R*-$TaSe_2$	NbS_2, $NbSe_2$, TaS_2, MoS_2, WS_2, ReS_2
$4H_{(a)}$-$TaSe_2$	$NbSe_2$
$4H_{(b)}$-$TaSe_2$	—
6*R*-$TaSe_2$	TaS_2

(ii) *The $Ta_{1+x}Se_2$ phase.* The composition range of the $Ta_{1+x}Se_2$ phase, estimated using the disappearing phase principle on the Guinier photographs, extends from ~55 to 66.7 ± 0.3 atomic % Se for samples cooled slowly from 900°C. The selenium-rich phase limit is favourable for determination according to this method since the polytypes of $TaSe_2$ are distinctly different crystallographically from the neighbouring phase $TaSe_3$.[15,16] An accurate estimation of the selenium-poor phase limit by this method is difficult due to the rather poor quality of the Guinier photographs of the samples with low selenium content.

The Guinier photographs of the $Ta_{1+x}Se_2$ phase were indexed in terms of unit cells corresponding to the polytypes of $TaSe_2$ (Tables 1—6). The lattice constants are listed in Table 8 for samples of various compositions. The dimensional variations of the unit cell(s) as a function of composition (Fig. 2) establish the homogeneity range as extending from 55.0 to 66.67 atomic % Se, *i.e.* $0.64 > x \geqq 0.00$ using the notation $Ta_{1+x}Se_2$. It should be mentioned, however, that a degree of uncertainty (<1 atomic % Se) is attached to the selenium-poor phase limit in order to allow for a possible concentration displacement resulting from the reaction between Ta and SiO_2.

The selenium-poor phase limit of 55.0 atomic % Se found in this study differs considerably from the value 50.00 atomic % Se reported by Ariya *et al.*[1] and Brixner.[3] However, neither Ariya *et al.* nor Brixner seem to have succeeded in the preparation of homogeneous $Ta_{1+x}Se_2$ samples since these authors observe an almost negligible change in lattice dimensions between 50.00 and 66.67 atomic % Se. The selenium-rich phase limits 66.44 and 65.75 atomic % Se reported by Aslanov *et al.*[5,6] and Quinn *et al.*[11], respectively, differ also to some extent from the value 66.67 atomic % Se obtained in this study.

It was difficult to obtain consistent, reproducible results within the homogeneity range, *i.e.* when $x > 0$, due to the close structural relationship between the possible polytypes (*cf.* Fig. 1). A large number of the samples within the concentration range of the $Ta_{1+x}Se_2$ phase contained a mixture of two or three of the polytypes. The most consistent results are obtained after relatively short heat treatment. Reannealing has generally not improved the samples, but has occasionally worsened the homogeneity. However, some general trends have been noticed for the occurrence of the different polytypes of $Ta_{1+x}Se_2$. The polytypes 1*T*, $4H_{(a)}$, $4H_{(b)}$, and 6*R* of $Ta_{1+x}Se_2$ have only

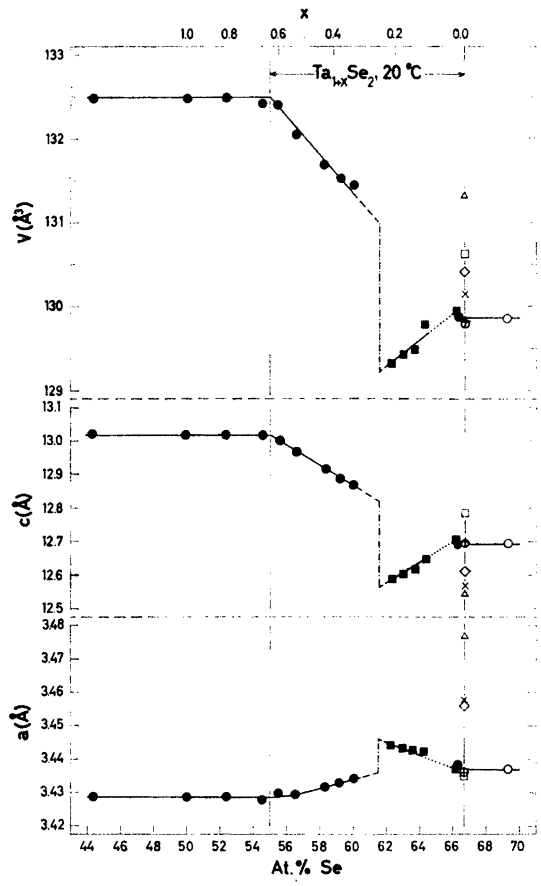

Fig. 2. Variations in lattice constants of the $Ta_{1+x}Se_2$ phase as functions of composition. (Results marked △ are for $1T$-$TaSe_2$, ○ for $2H$-$TaSe_2$, ● for $2H$-$Ta_{1+x}Se_2$ with $x > 0$, □ for $3R$-$TaSe_2$, ■ for $3R$-$Ta_{1+x}Se_2$ with $x > 0$, + for $4H_{(a)}$-$TaSe_2$, × for $4H_{(b)}$-$TaSe_2$, and ◇ for $6R$-$TaSe_2$.)

been obtained for $x = 0.00$. Samples containing pure $2H$-$Ta_{1+x}Se_2$ have been obtained for $0.00 \leqq x < 0.03$ and $0.25 < x < 0.64$ (Table 8 and Fig. 2). $3R$-$Ta_{1+x}Se_2$ have been observed for $0.03 < x < 0.25$, however, almost invariably mixed with traces of $2H$-$Ta_{1+x}Se_2$.

The relationships between the different polytypes of the $Ta_{1+x}Se_2$ phase are governed not only by thermodynamics, as was first pointed out by Kadijk *et al.*[8] The current theory for the formation of polytype phases assumes that polytypism results from the spiral growth of crystals, initiated by screw dislocations. A discussion of the occurrence of polytypes of the $Ta_{1+x}Se_2$ phase on this basis has been given Selte *et al.*[2] and reference is made to the latter paper for further details (see also Kadijk *et al.*[8] and Jellinek [14]).

The dimensional variations of the unit cells as function of composition are shown in Fig. 2. The dimensions of the c axes for the polytypes $1T$, $3R$, $4H_{(a)}$, $4H_{(b)}$, and $6R$ have been converted to match the c axis of the polytype $2H$-$Ta_{1+x}Se_2$ in this diagram. Several interesting features are seen on considering the changes in the a and c axes as functions of composition (Fig. 2). An apparently discontinuous change in the a and c parameters of the structures is to be noticed in the region $\sim 60 - \sim 62$ atomic % Se. It should be noted, however, that the two portions of the curves correspond to two different polytypes. The lattice constants of both polytypes vary as approximately linear functions of composition, but in a reverse manner for the two axes and the two polytypes. Considering, *e.g.*, the a (axis) curves in Fig. 2, the slope for $2H$-$Ta_{1+x}Se_2$ is approximately equal to, but of opposite sign to that for $3R$-$Ta_{1+x}Se_2$ whereas the two curve-portions extrapolate to approximately the same value for $x = 0.00$. A similar observation is made for the c parameter in Fig. 2. It is also recognized that for $3R$-$Ta_{1+x}Se_2$ a expands and c contracts with increasing Ta content. (*Vice versa* for $2H$-$Ta_{1+x}Se_2$.) This contraction of c may be regarded as being complementary to the expansion of a thus reducing the change in cell volume. However, the percentage variations in c are more than one order of magnitude larger than the corresponding variations in a and the cell volume V *versus* composition relationship resembles accordingly that of c.

A series of density measurements was carried out in order to confirm the formula $Ta_{1+x}Se_2$. Good agreement was obtained by comparison of the pycnometrically observed densities with those calculated on the basis of the structural data in Table 8 for samples with composition corresponding to $x = 0.00$. ($1T$-$TaSe_2$: $d_{pycn} = 8.503$ gcm^{-3}, $d_{X\text{-}ray} = 8.569$ gcm^{-3}; $2H$-$TaSe_2$: $d_{pycn} = 8.679$ gcm^{-3}, $d_{X\text{-}ray} = 8.669$ gcm^{-3}; $3R$-$TaSe_2$: $d_{pycn} = 8.599$ gcm^{-3}, $d_{X\text{-}ray} = 8.614$ gcm^{-3}; $4H_{(a)}$-$TaSe_2$: $d_{pycn} = 8.606$ gcm^{-3}, $d_{X\text{-}ray} = 8.665$ gcm^{-3}. Quantities sufficient for density measurements of the pure polytypes $4H_{(b)}$-$TaSe_2$ and $6R$-$TaSe_2$ were not obtained.) For samples with composition corresponding to $x > 0$ the observed densities are 2—6 % lower than those calculated from the structural data assuming the formulae $2H$-$Ta_{1+x}Se_2$ and $3R$-$Ta_{1+x}Se_2$. The lower values of the observed densities are easily explained making the reasonable assumption that these samples contain impurities (of relatively low density) resulting from the reaction between Ta and SiO_2 (see Experimental). Although the density measurements are of limited value in proving the addition hypothesis the general tendency of the results indicates the correctness of the formula $Ta_{1+x}Se_2$.

The structures of all the $TaSe_2$ polytypes have vacant positions (see Fig. 1 and Table 7) which can accommodate the additional metal atoms. The available empty positions, indicated by crosses in Fig. 1, are of the octahedral type in all the structure types. Single crystals of $Ta_{1+x}Se_2$ with $x > 0$ were unfortunately not obtained and preferred orientation on the sample holder renders the use of intensities collected from powder photographs more or less meaningless for accurate structure confirmations.

The coordination around the Ta and Se atoms in the various structures can be seen from Fig. 1, and the shortest interatomic distances (calculated on the basis of the structural data listed in Tables 7 and 8) are given in Table 10.

The variation of the interatomic Ta-Se distance between nearest neighbours (trigonal prismatic and/or octahedral coordination) as a function of composition (Fig. 3) resembles (as expected) the corresponding variation of the c parameter in Fig. 2.

(iii) Magnetic properties. The magnetic susceptibilities of $1T$-$TaSe_2$, $2H$-$TaSe_2$, $3R$-$TaSe_2$, and $4H_{(a)}$-$TaSe_2$ were measured between 90 and 725°K

Table 10. Interatomic distances in $Ta_{1+x}Se_2$ (Å).

x	Poly-type	Ta-xTa	Ta-6Ta	Ta-6Se	Se-(3+3x)Se	Se-1Se	Se-6Se	Se-3Se
0.00	$1T$	—	3.477	2.54_7	2.54_7	—	3.477	3.72_4
0.00	$2H$	—	3.436	2.54_1	2.54_1	3.174	3.436	3.74_3
0.00	$3R$	—	3.435	2.54_7	2.54_7	3.196	3.435	3.76_1
0.00	$4H_{(a)}$	—	3.436	2.54_1	2.54_1	3.175	3.436	3.74_4
0.00	$4H_{(b)}$	—	3.458	2.54_1	2.54_1	3.143	3.458	3.72_3
0.00	$6R$	—	3.456	2.54_3	2.54_3	3.152	3.456	3.73_1
0.02	$2H$	3.174	3.437	2.54_1	2.54_1	3.174	3.437	3.74_3
0.03	$3R$	3.176	3.437	2.54_2	2.54_2	3.176	3.437	3.74_5
0.11	$3R$	3.163	3.442	2.54_0	2.54_0	3.163	3.442	3.73_5
0.14	$3R$	3.154	3.443	2.53_7	2.53_7	3.154	3.443	3.72_8
0.18	$3R$	3.151	3.444	2.53_7	2.53_7	3.151	3.444	3.72_6
0.21	$3R$	3.147	3.444	2.53_6	2.53_6	3.147	3.444	3.72_3
0.33	$2H$	3.218	3.434	2.55_3	2.55_3	3.218	3.434	3.78_0
0.38	$2H$	3.222	3.433	2.55_4	2.55_4	3.222	3.433	3.78_3
0.43	$2H$	3.229	3.432	2.55_6	2.55_6	3.229	3.432	3.78_8
0.54	$2H$	3.241	3.429	2.55_8	2.55_8	3.241	3.429	3.79_8
0.60	$2H$	3.249	3.430	2.56_1	2.56_1	3.249	3.430	3.80_5

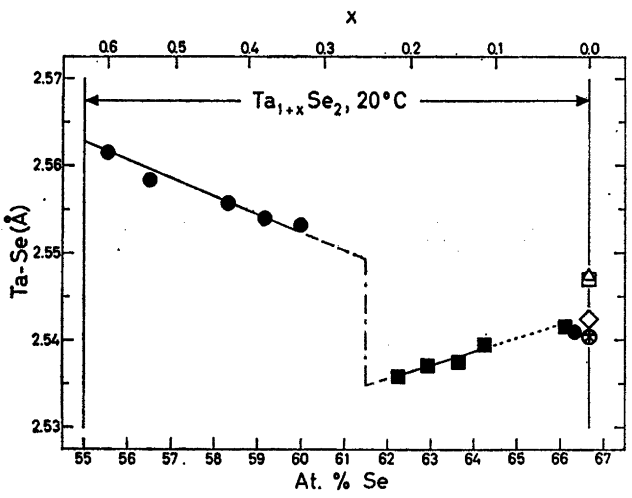

Fig. 3. The shortest interatomic Ta-Se distance in $Ta_{1+x}Se_2$ as a function of composition (see caption to Fig. 2).

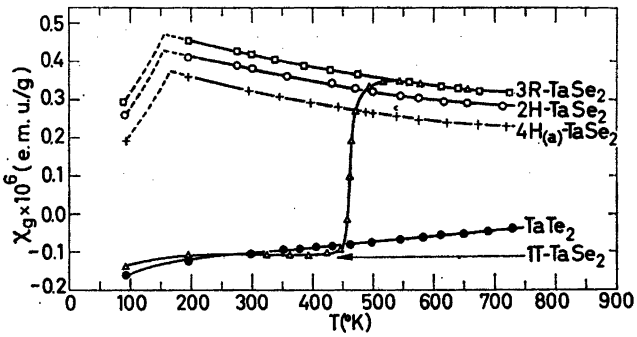

Fig. 4. Magnetic susceptibilities of $1T$-$TaSe_2$, $2H$-$TaSe_2$, $3R$-$TaSe_2$, $4H_{(a)}$-$TaSe_2$, and $TaTe_2$ as functions of temperature.

and the results are shown in Fig. 4. (Our unpublished data for $TaTe_2$ have also been included in this diagram.) Field strength dependent susceptibilities were not observed, and mean values of the susceptibilities at the various field strengths are therefore given in Fig. 4. The experimental curves have not been corrected for induced diamagnetism. The expected diamagnetism resulting from the atomic cores was calculated from the diamagnetic corrections -14×10^{-6} e.m.u. per mole Ta^{5+} (according to Klemm [17]) and -47.6×10^{-6} e.m.u. per mole Se^{2-} (according to Angus [18]) and amounts to -0.32×10^{-6} e.m.u. per gram $TaSe_2$. (The core contribution is -0.36×10^{-6} e.m.u. per gram $TaTe_2$.) By subtracting these values from the measured susceptibilities, the total susceptibilities of localized, non-bonding electrons, valence electrons, and conduction electrons are obtained.

Diamagnetic susceptibility is found for $1T$-$TaSe_2$ (and $TaTe_2$). The transformation of $1T$-$TaSe_2$ into $3R$-$TaSe_2$ (see section i) between ~450 and ~500°K is clearly reflected in the magnetic susceptibility *versus* temperature curves of the two polytypes.

$2H$-$TaSe_2$, $3R$-$TaSe_2$, and $4H_{(a)}$-$TaSe_2$ show paramagnetic susceptibilities. The temperature dependences of the magnetic susceptibilities of these polytypes indicate that the Curie-Weiss law is almost satisfied above ~200°K, whereas below this temperature the curves indicate transitions to antiferromagnetic states. A moment of about 2.1 B.M. per Ta atom (for each of the three polytypes) is obtained on application of the diamagnetic correction stated above. The "spin only" approximation would demand a magnetic moment of 1.73 B.M. for one unpaired electron per Ta atom. The higher value observed can be accounted for by assuming a contribution from an unquenched orbital angular momentum. However, the possible inaccuracy in the diamagnetic corrections hardly justifies a detailed discussion of this discrepancy.

The values for Néel temperature and magnetic moment found in this study compare fairly well with $T_N \approx 130$°K and $\mu \approx 2.4$ B.M. reported by Quinn *et al.*[11] for $2H$-$Ta_{1+x}Se_2$. One further comment regarding the results

of Quinn *et al.* for $2H$-$Ta_{1+x}Se_2$ seems to be appropriate. The thermo-magnetic curves in their Fig. 3 show an apparently anomalous and sudden change from paramagnetism to diamagnetism at ~1150°K. The observed diamagnetism for $1T$-$TaSe_2$ (see Fig. 4) and the formation and thermal stability of this polytype above ~900°C (see section i) appear to give a sufficient explanation of this anomaly. (The c axis of the $TaSe_{1.92}$ sample examined by Quinn *et al.* at 1200°K can clearly be halved since the diffraction data in their Table I only include reflections having an even value for the index l.).

Acknowledgement. The authors wish to thank Professor Haakon Haraldsen for his kind interest in this study and for placing laboratory facilities at their disposal.

REFERENCES

1. Ariya, S. M., Zaslavskii, A. I. and Matveeva, I. I. *Zh. Obshch. Khim.* **26** (1956) 2373.
2. Selte, K., Bjerkelund, E. and Kjekshus, A. *J. Less-Common Metals* **11** (1966) 14.
3. Brixner, L. H. *J. Inorg. Nucl. Chem.* **24** (1962) 257.
4. Brixner, L. H. *J. Electrochem. Soc.* **110** (1963) 289.
5. Aslanov, L. A., Ukrainskii, Yu. M. and Simanov, Yu. P. *Russian J. Inorg. Chem. (English Transl.)* **8** (1963) 937.
6. Aslanov, L. A., Simanov, Yu.P., Novoselova, A. V. and Ukrainskii, Yu. M. *Russian J. Inorg. Chem. (English Transl.)* **9** (1964) 1224.
7. Boes, D. J. *IEEE Trans. Aerospace* **2** (1964) 457.
8. Kadijk, F., Huisman, R. and Jellinek, F. *Rec. Trav. Chim.* **83** (1964) 768.
9. Brown, B. E. and Beerntsen, D. J. *Acta Cryst.* **18** (1965) 31.
10. Revolinsky, E., Brown, B. E., Beerntsen, D. J. and Armitage, C. H. *J. Less-Common Metals* **8** (1965) 63.
11. Quinn, R. K., Simmons, R. and Banewicz, J. J. *J. Phys. Chem.* **70** (1966) 230.
12. Swanson, H. E. and Tatge, E. *Natl. Bur. Std. (U.S.) Circ.* 539 I (1953), p. 29.
13. Hambling, P. G. *Acta Cryst* **6** (1953) 98.
14. Jellinek, F. *Arkiv Kemi* **20** (1963) 447.
15. Bjerkelund, E. and Kjekshus, A. *Z. anorg. allgem. Chem.* **328** (1964) 235.
16. Bjerkelund, E. and Kjekshus, A. *Acta Chem. Scand.* **19** (1965) 701.
17. Klemm, W. *Z. anorg. allgem. Chem.* **246** (1941) 347.
18. Angus, W. R. *Proc. Roy. Soc. (London)* **A 136** (1932) 569.

Received October 25, 1966.